Chapter 18

Coarse-Grained Molecular Dynamics Simulations of the Bacterial Cell Wall

Lam T. Nguyen, James C. Gumbart, and Grant J. Jensen

Abstract

Understanding mechanisms of bacterial sacculus growth is challenging due to the time and length scales involved. Enzymes three orders of magnitude smaller than the sacculus somehow coordinate and regulate their processes to double the length of the sacculus while preserving its shape and integrity, all over a period of tens of minutes to hours. Decades of effort using techniques ranging from biochemical analysis to microscopy have produced vast amounts of data on the structural and chemical properties of the cell wall, remodeling enzymes and regulatory proteins. The overall mechanism of cell wall synthesis, however, remains elusive. To approach this problem differently, we have developed a coarse-grained simulation method in which, for the first time to our knowledge, the activities of individual enzymes involved are modeled explicitly. We have already used this method to explore many potential molecular mechanisms governing cell wall synthesis, and anticipate applying the same method to other, related questions of bacterial morphogenesis. In this chapter, we present the details of our method, from coarse-graining the cell wall and modeling enzymatic activities to characterizing shape and visualizing sacculus growth.

Key words Coarse-grained modeling, Molecular dynamics simulations, Cell wall synthesis, Bacterial morphogenesis, Rod shape maintenance

1 Introduction

Most bacterial cells are surrounded by a sacculus that prevents lysis from turgor pressure and determines the cell's shape (e.g., a rod, in the case of *E. coli*) [1]. How the cell coordinates sacculus growth so that breaks introduced to allow insertion of new material do not cause lysis remains an open question.

Considerable work has revealed the structure of the sacculus. Paper chromatography and high-performance liquid chromatography (HPLC) revealed that the *E. coli* sacculus is made of peptidoglycan (PG) [2–4]. The glycan strand is polymerized from disaccharides of an *N*-acetylglucosamine (NAG) and an *N*-acetylmuramic (NAM) acid, each attached to a stem L-Ala-D-iGlu-m-A_2pm-D-Ala-D-Ala penta-peptide. Peptides on adjacent strands form crosslinks, most at

Hee-Jeon Hong (ed.), *Bacterial Cell Wall Homeostasis: Methods and Protocols*, Methods in Molecular Biology, vol. 1440,
DOI 10.1007/978-1-4939-3676-2_18,

the fourth (D-Ala) residues of the donors and the third (m-A_2pm) residues of the acceptors, resulting in a mesh-like PG network. Early electron microscopy studies revealed that purified sacculi retain the cell's rod shape [5]. Later, electron cryo-tomography was used to show that glycan strands run circumferentially around the rod [6]. This is consistent with a classical model of sacculus architecture which posits that long and stiff glycan strands run circumferentially, bearing the greatest stress, while short and flexible peptide crosslinks run parallel to the rod's long axis, bearing half as much stress [1].

Other work revealed the enzymatic details of the PG synthesis machinery. PG precursors are synthesized in the cytoplasm and then transferred to the periplasm [7] where they are polymerized and crosslinked into the sacculus by transglycosylases and transpeptidases, also known as penicillin-binding proteins (PBPs) [8]. Also essential to the process are endopeptidases that cleave covalent bonds to open space for the new material [9]. X-ray crystallography has revealed the structures of many synthases and hydrolases from multiple species [8, 10], and the enzymatic activities of *E. coli* synthases have been characterized in vitro [11, 12]. Affinity chromatography and bacterial two-hybrid studies showed that many synthases and hydrolases interact with one another [12–16] and with the outer membrane proteins LpoA/B [17, 18], suggesting that the enzymes exist in a complex spanning the periplasm. While affinity chromatography showed that both cytoplasmic and periplasmic enzymes interact with the morphogenetic proteins MreB/C/D and Rod A/Z [19–21], fluorescence microscopy has yielded conflicting results as to whether these proteins co-localize/move in the same complex [21–25].

Despite decades of experiments, how the activities of PG synthesis enzymes are coordinated at the molecular and cellular levels remains unclear. Several models have been proposed. For instance, a "make-before-break" strategy was proposed in which autolysins would cleave crosslinks along the template strand to liberate it only after new strands are fully crosslinked to the sacculus underneath the existing strand, thus preventing lysis [26]. Whether the enzymes could actually be coordinated to execute such temporally and spatially separated operations is unclear, however. Similarly, it was proposed that the cytoskeletal protein MreB forms an extended filament that guides PG insertion to maintain rod shape [27]. Disagreement on the oligomeric form and driving force of movement of MreB [23, 24, 27–41], however, obscures its role in PG synthesis.

We realized that another approach is needed to shed light on the coordination of PG remodeling enzymes. Coarse-grained simulation of cell wall remodeling, pioneered by Huang and colleagues [42], has proven to be a valuable method to test different models suggested by experiments. The Huang model, however, has mainly focused on different mechanisms by which MreB might guide insertion sites of new PG. To do that, the incorporation of each

new PG strand into the sacculus has been modeled as a single event in which an entire glycan strand is introduced, and all necessary peptide crosslinks cleaved and re-formed, all in one step before any relaxation of the sacculus can occur [28, 41, 43, 44]. This reduces the computational cost but has prevented an exploration of the properties and coordination of PG remodeling enzymes.

In order to explore different molecular mechanistic models of sacculus growth, we have developed a simulation method that allows us to vary properties of PG-remodeling enzymes and their coordination [45]. To make our model as realistic as possible, PG is represented by a coarse-grained model whose mechanical properties were derived from all-atom molecular dynamics (MD) simulations of isolated glycan strands and peptides. For the first time to our knowledge, individual enzymes, including transglycosylases, transpeptidases, and endopeptidases, are explicitly represented.

The rich literature of biochemical data and hypothetical models made it challenging to build our initial model. One approach would have been to implement all the models proposed in the literature. Many models, however, are contradictory, e.g., multienzyme complex [46] vs. diffusive transpeptidase [25], extended helical MreB filament [27, 29–35] vs. circumferentially moving MreB spots [23, 24, 28], or single-strand insertion [47, 48] vs. strands inserted in pairs [49–52]. And even if the combined models worked, it would be impossible to dissect which models are required and which redundant. We instead decided to pursue the simplest model that works. We started with a very simple model (named Remodeler 1.0, as explained below) and implemented additional hypotheses only when necessary. A schematic of this process is presented in Fig. 1, and readers are referred to [45] for details. For each model that failed to maintain rod shape, we

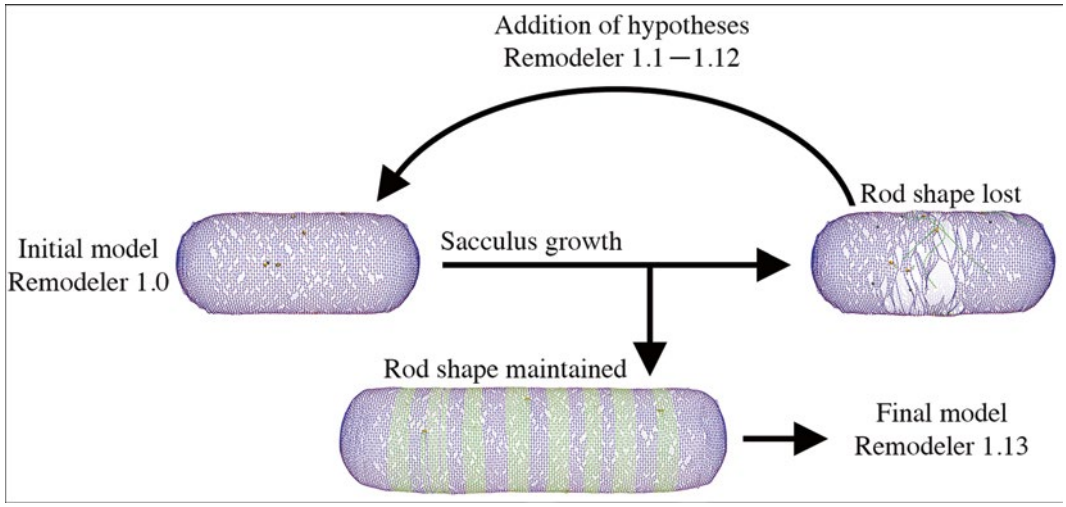

Fig. 1 Schematic of the process of iteratively building a complex model from a simple initial model

analyzed the most obvious cause and added a molecular hypothesis based on evidence from the literature and/or biophysical plausibility to fix the problem. This process was iterated until rod shape was maintained (Remodeler 1.1–1.12). Finally, we removed hypotheses one by one from Remodeler 1.12 to check if any were rendered redundant by the other hypotheses. The final model (Remodeler 1.13) thus comprised one simple set of hypotheses capable of maintaining rod shape during sacculus growth.

We have used our model to study how rod shape might be maintained in Gram-negative bacteria (*see* **Note 1**). We distributed the simulation codes for each stage of this model, named Remodeler 1.0–1.13 [45]. In the future, we anticipate further developing our model to study other PG-synthesis related topics, from rod shape maintenance in Gram-positive bacteria, to shape recovery of perturbed cells, to cell division and even sporulation (*see* **Note 2**). In each case, we will name our models Remodeler 2.x, 3.x, and so on to help readers who wish to use our codes, starting with any stage of the model.

In the following sections, the details of our model are described and a brief discussion of results is presented. Readers are advised to watch https://www.youtube.com/watch?v=_5Ov3vp6Qyg&feature=youtu.be since video represents the model building process better than static figures. For further details of results and discussion, the readers are referred to [45].

2 Materials

All-atom MD simulations were conducted using the software NAMD [53]. The coarse-grained simulation software was written using Fortran language. Visualization of simulation data was done using Visual Molecular Dynamics (VMD) [54]. Images were processed using Photoshop. Movies were made using QuickTime Pro and concatenated using Final Cut Pro.

3 Method

The general procedure for sacculus growth simulations is illustrated in Fig. 2. First (Setup), we built the initial system, composed of a sacculus and a set of enzymes including transglycosylases, transpeptidases, and endopeptidases. Next (PG remodeling), in each time step, each enzyme performed its function with a certain probability. Forces exerted on the sacculus and enzymes were then calculated and the coordinates of the system updated (PG relaxation). The process of PG remodeling and relaxation was repeated until the sacculus reached the desired mass. We discuss the details of the procedure below.

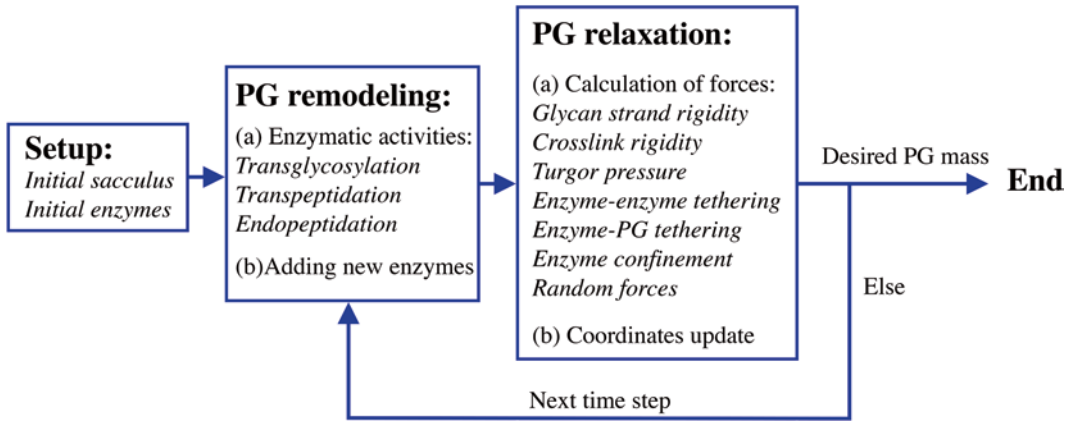

Fig. 2 Computational procedure for sacculus growth. For clarity, the names of code sections are italicized in all flowcharts

3.1 Coarse-Grained Peptidoglycan Model

Most MD simulation software provides atomic-level insights into processes that occur on the nanosecond timescale; for example, NAMD was used to simulate an HIV-1 capsid of ~10^7 atoms over a period of ~500 ns [55]. By contrast, the sacculus is a giant molecule (on the order of 10^8 atoms) that doubles its size over a period of minutes to hours. Coarse-graining the sacculus helps reduce the computational cost, allowing observation of phenomena occurring at both the molecular and cellular levels. To do this, we represented each pair of disaccharides as one bead and connected the beads with springs to form chain-like glycan strands. As adjacent disaccharides are rotated 90° with respect to each other [56–58], half of the peptides presumably protrude perpendicular to the sacculus surface and do not participate in crosslinking. We therefore ignored these out-of-plane peptides. Thus, each bead in our coarse-grained model was attached to one in-plane peptide (Fig. 3a).

3.1.1 Glycan Mechanical Properties

We previously developed all-atom force fields for PG [59, 60] that allowed us to set the mechanical properties of the coarse-grained model to match the behavior of all-atom MD simulations. To calculate the stiffness of glycan, a fully solvated system of an 80-tetrasaccharide strand without stem peptides was equilibrated for 6.6 ns using the software NAMD [53] (Fig. 3b). For scale, this system contained nearly one million atoms (mostly solvent) and was over 150 nm in length, yet represents only a miniscule fraction of the entire sacculus. During the simulation, the strand shrank slightly, by about 2%, but maintained an extended conformation overall. We then extracted histograms of distances and bending angles between adjacent tetrasaccharides. MD simulations were next run on an equivalently sized coarse-grained (CG) strand where adjacent beads, each representing one tetrasaccharide, were connected by springs of constant k_g and relaxed length l_g, and a bending angle θi at bead i was penalized with an energy of

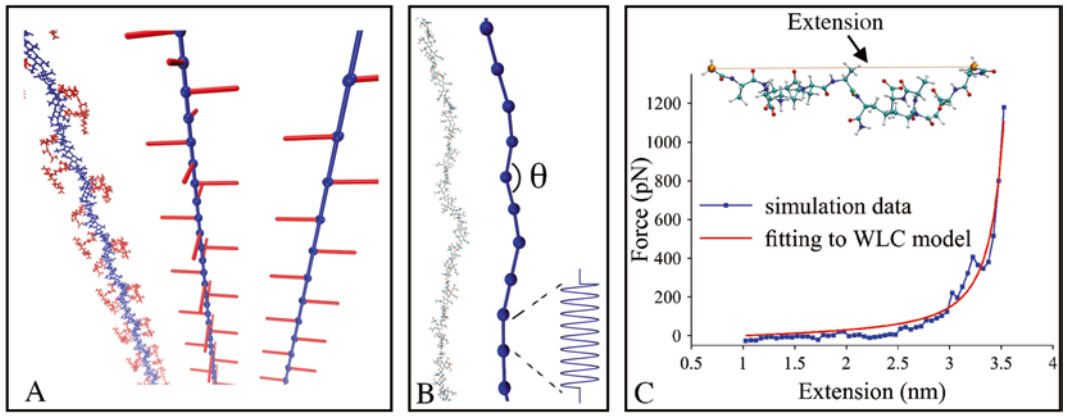

Fig. 3 Parameterization of the coarse-grained model, adapted from [45]. (**a**) The glycan strand—disaccharides in *blue* and peptides in *red*—in atomic representation (*left*) was coarse-grained as a chain of beads, each representing first a disaccharide attached to a peptide (*middle*) and finally a tetrasaccharide attached to an in-plane peptide (*right*). (**b**) Snapshots of a glycan strand in all-atom MD (*left*) and coarse-grained simulations (*right*). In the latter, the strand was modeled as a chain of beads connected by springs. (**c**) Extension dependence of force on a peptide crosslink extracted from all-atom MD simulations (*blue*), and after fitting to a worm-like chain model (*red*)

$$E_{\mathrm{b}}^{(i)} = \frac{1}{2} k_{\mathrm{b}} \left(\theta_i - \theta_0\right)^2 \tag{1}$$

where k_{b} is the bending stiffness and θ_0 is the relaxed angle. A Langevin damping term of $\gamma = 2\mathrm{ps}^{-1}$ was added to mimic water viscosity; values ranging from 1 to 5 ps^{-1} were tested and found to have no effect on the resulting sampled bond and angle lengths. A time step of 100 fs was used for the CG simulations and they were run for 500 ns (note that times are not directly comparable between the simulations due to the significantly simplified potential of CG simulations). The parameters for the CG model were iteratively sampled until the histograms extracted from CG simulations matched those of the all-atom simulations by visual inspection. The CG parameters that produced the best match were $k_{\mathrm{g}} = 5570$ pN/nm, $l_{\mathrm{g}} = 2.0$ nm, $k_{\mathrm{b}} = 8.36 \times 10^{-20}$ J, and (as expected) $\theta_0 = 3.14$ rad.

3.1.2 Peptide Crosslink Mechanical Properties

Initially, we tried to fit the peptide-crosslink bond strength using a similar histogram matching procedure. However, it quickly became apparent that no match could be obtained; the bond-distance histogram from the atomistic simulations of three crosslinked glycan strands was not symmetric as would be expected for a harmonic bond. To better understand the length distribution of peptide crosslinks, we simulated a single peptide crosslink, i.e., an Ala(1)-isoGlu(2)-A_2pm(3)-Ala(4)-Ala(5) pentapeptide linked to an Ala(1)-isoGlu(2)-A_2pm(3)-Ala(4) tetrapeptide through an A_2pm(3)-Ala(4) peptide bond. Specifically, we determined the potential of mean

force (PMF) as a function of end-to-end extension. We used all-atom MD adaptive biasing force (ABF) simulations so the full energy landscape could be assessed quickly. This is a quasi-equilibrium method in which the biasing forces exerted on the two terminal (reaction) atoms are iteratively calculated as the *positive* gradient of the PMF, thus making the two atoms diffuse freely [61, 62]. The reaction coordinate (extension) was divided into four 10-Å windows to accelerate convergence; each was run for between 5 and 8 ns. Based on the resulting PMF and associated mean-force profile, we determined that the peptide crosslink is better modeled as a worm-like chain (WLC) than a spring, i.e., the force is almost zero at small extension, increases only moderately for extensions less than the contour length, but then increases dramatically at large extension (Fig. 3c). We therefore fit the mean force vs. extension curve to the following formula:

$$F\left(x^*\right) = k_{\mathrm{WLC}}\left[\frac{L_c^*}{4\left(1 - x^* / L_c^*\right)^2} - \frac{L_c^*}{4} + x^*\right] \tag{2}$$

where $L_c^* = L_c - x_0$ is the effective contour length, L_c is the contour length, x_0 is the extension (end-to-end distance) x at which the force is zero, $x^* = x - x_0$ is the effective extension, and k_{WLC} is a force constant. We then determined the parameters that produced the best fit as $k_{\mathrm{WLC}} = 15.0$ pN/nm, $L_c = 4.8$ nm, and $x_0 = 1.0$ nm (*see* **Note 3**). Consistently, Braun et al. used space-filling models to show that the peptide crosslink is ~4.2 nm long when fully extended and ~1.0 nm long when maximally collapsed [63], which agrees well with the L_c and x_0 derived from our simulations.

3.1.3 Initial Sacculus

The initial sacculus model was built by placing glycan strands along circumferential hoops (Fig. 4a) and connecting opposing peptides on adjacent hoops to form crosslinks (Fig. 4b). We used hoops of the same diameter to form a cylindrical waist, and those of gradually decreasing diameter to form two polar caps. Initially, the lengths of glycan strands were chosen uniformly randomly within a range from 10 to 20 tetrasaccharides (later, during sacculus growth, the length was determined by the enzyme processivity). To reduce the computational cost, we used an initial sacculus of circumference 100 tetrasaccharides, ~10 times smaller than typical wild-type *E. coli* cells. We did, however, test the effect of size by running simulations on sacculi of diameters twice and four times as large (about the size of a small rod-shaped Gram-negative cell such as *Acetonema longum*), and obtained similar results [45] (*see* **Note 4**).

Note that even though the initial sacculus was built with ordered glycan strands, its shape after relaxation in the presence of turgor pressure is a function of the mechanical properties of glycan strands and peptide crosslinks.

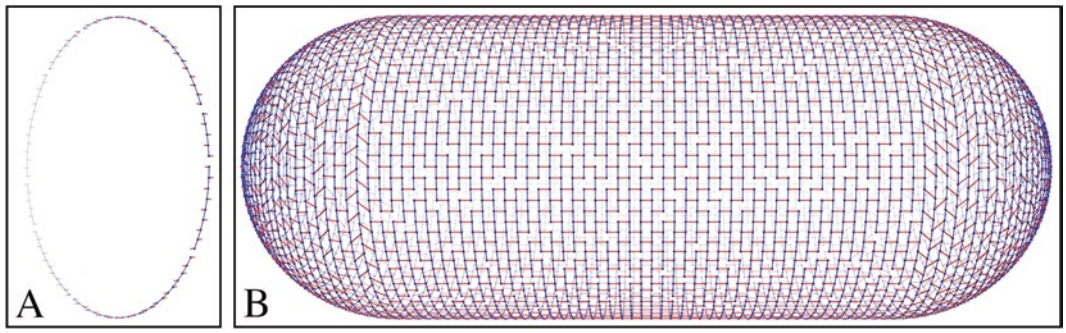

Fig. 4 Building a coarse-grained sacculus. (**a**) Coarse-grained glycan strands were arranged in hoops. (**b**) A sacculus was formed by connecting peptides on adjacent hoops

3.2 Turgor Pressure

Turgor pressure plays an important role in sacculus growth as it inflates the sacculus, allowing new material to be incorporated. We therefore added to the total energy of the system the work done by turgor pressure P to inflate the sacculus to volume V:

$$E_{\text{vol}} = -PV \tag{3}$$

To calculate V, the volume enclosed by the sacculus, the mesh-like surface was divided into a series of polygons (Fig. 5). The polygons were then further divided into triangles from which tetrahedrons were built using the sacculus center as the fourth vertex. V was then calculated as the sum volume of the tetrahedrons:

$$V = \sum_i V_i = \sum_i A_i h_i / 3 \tag{4}$$

where Ai is the area of triangle i and hi is the distance from the sacculus center to the plane of triangle i. The force on the sacculus due to turgor pressure was then calculated as $F = -\nabla E_{\text{vol}}$. As most measurements of turgor pressure within Gram-negative bacteria have been reported to be between 2 and 4 atm [64–66], we used a turgor pressure of 3.0 atm in most of our simulations.

3.3 Coarse-Grained Model of Enzymes

While current MD simulation software is limited to the study of "closed" systems, our coarse-grained model allows exploration of "open" systems by implementing enzymatic activities that could add or remove beads and bonds. To explore possible molecular mechanisms of PG synthesis, generic transglycosylases, transpeptidases, and endopeptidases were modeled explicitly as individual coarse-grained beads (Fig. 6). They were modeled to diffuse within the confines of the periplasm and interact with each other and with the sacculus while performing their functions. By modeling enzymatic activities step-by-step, we could investigate different molecular mechanisms for spatial and temporal coordination of the enzymes.

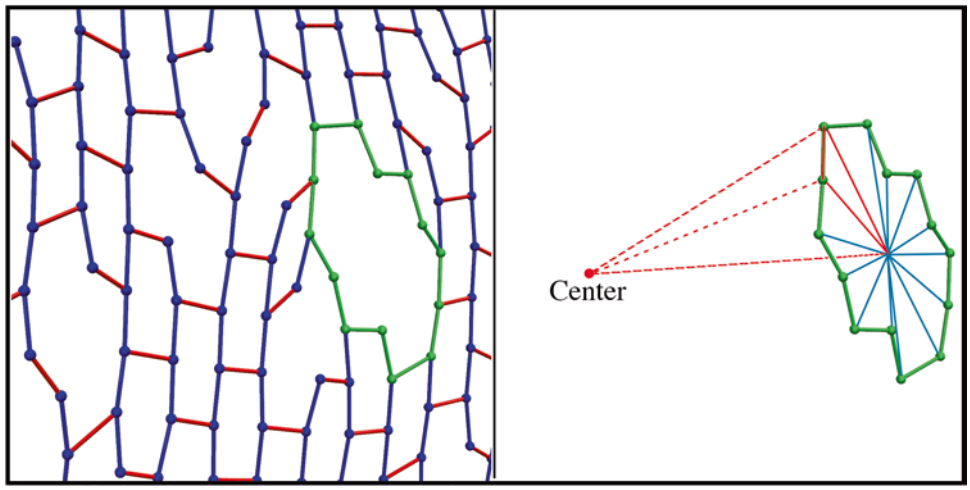

Fig. 5 Volume determination. A polygon (*green*) on the sacculus surface (*left*) was divided into triangles, each having an edge on the polygon and sharing the polygon's center as the third vertex (*right*). Tetrahedrons were then built from the triangle using the sacculus center as the fourth vertex

Note that in our later simulations, glycosidic bond hydrolysis and carboxypeptidation were also implemented without explicitly modeling the corresponding enzymes [45].

We implemented stepwise enzymatic activities using flags, which we capitalize for clarity in the following descriptions. Each enzymatic activity was modeled to occur with a probability that was arbitrarily chosen since we were unaware of any biochemical data on the rates of PG synthesis enzymes in vivo.

3.3.1 Transglycosylation

For *transglycosylation*, the enzymes were modeled as INACTIVE (not synthesizing but diffusing around) or ACTIVE (ready to synthesize a new strand). ACTIVE transglycosylases were modeled as STRAND-FREE (not holding a new strand), STRAND-BOUND (donor domain holding a new strand), PRECURSOR-FREE (not loaded with a precursor in the acceptor domain), or PRECURSOR-LOADED (loaded with a precursor in the acceptor domain). STRAND-BOUND enzymes could be PRE-TRANSLOCATED (immediately after initiating a new strand or adding a bead to the growing strand), or TRANSLOCATED (translocated to the strand tip after initiating a new strand or adding a new bead to the growing strand, ready to be loaded with a precursor). A flowchart of the *transglycosylation* loop in our simulation code is presented in Fig. 7.

An INACTIVE transglycosylase, upon interaction with a lipoprotein was "activated" with a probability of once every 10^4 steps. ACTIVE but STRAND-FREE transglycosylases became STRAND-BOUND once they were "loaded" with a PG precursor bead in the active site (Fig. 6). Precursor loading was modeled to occur with a probability of once every 10^3 time steps. Precursor reloading on a

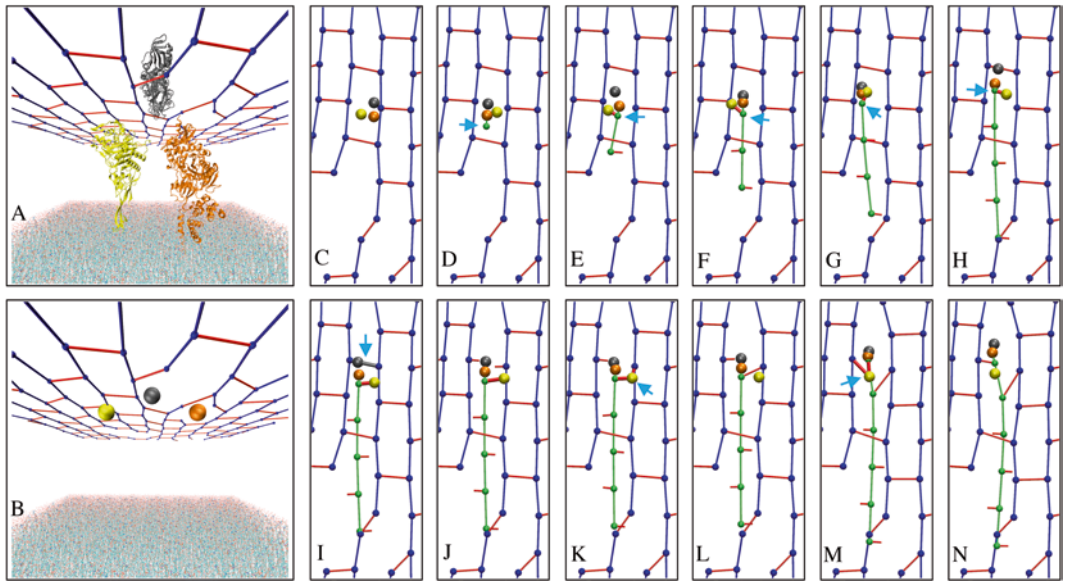

Fig. 6 Coarse-grained model of enzymes. A transglycosylase (3FWM, [10]) in *orange*, a transpeptidase (3EQV, [85]) in *yellow*, and an endopeptidase (2EX2, [86]) in *gray* are shown in crystal structures (**a**), and modeled as beads (**b**). Inner membrane is shown for context. (**c**–**n**) Visual depiction of enzymatic activities (noted by *blue arrows*). A transglycosylase initiates a new strand (shown in *green*) (**d**), and elongates it (**e**–**h**). An endopeptidase cleaves a peptide crosslink (**i**). A transpeptidase crosslinks the new strand to the sacculus (**k**, **m**)

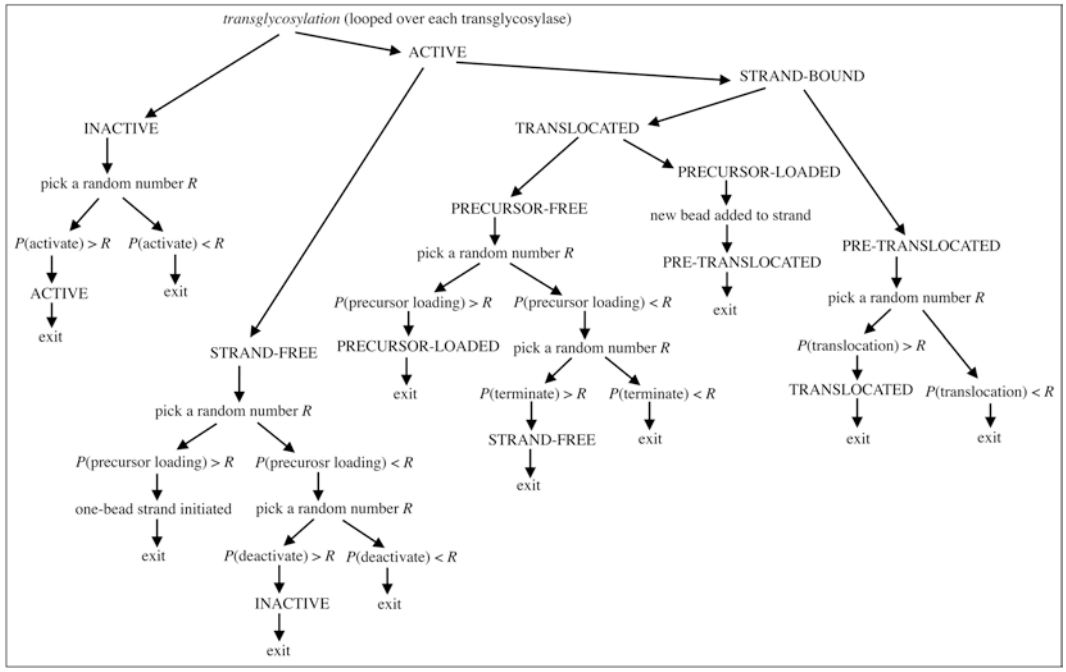

Fig. 7 Flowchart of *transglycosylation* in the simulation code. P denotes probabilities of the activities in a time step

STRAND-BOUND enzyme was prohibited until the enzyme TRANSLOCATED to the strand tip [67–69], which occurred with a probability of once every 2×10^4 time steps. A TRANSLOCATED transglycosylase could either be reloaded with another precursor, leading to further strand elongation (Fig. 6), or termination could occur, with a probability of once every 10^6 steps, leaving the transglycosylase once again in an ACTIVE but STRAND-FREE state. While an ACTIVE, STRAND-FREE transglycosylase could initiate a new strand, it could also be "inactivated," with a probability of once every 5×10^4 steps.

3.3.2 *Transpeptidation*

It is widely accepted that transpeptidation occurs in an ordered fashion in which the enzyme first binds to a donor peptide, forming an intermediary complex which later catalyzes crosslink formation when an acceptor peptide is captured [70–72]. Transpeptidases were therefore modeled to be either DONOR-FREE (not loaded with a peptide in the donor domain) or DONOR-LOADED (loaded with a peptide in the donor domain). DONOR-LOADED enzymes could exist as either ACCEPTOR-FREE (not loaded with a peptide in the acceptor domain) or ACCEPTOR-LOADED (loaded with a peptide in the acceptor domain).

A flowchart of the *transpeptidation* loop in the simulation code is presented in Fig. 8. A DONOR-FREE transpeptidase within a reaction distance, $d_0 = 2.0$ nm, of a bead bearing an uncrosslinked

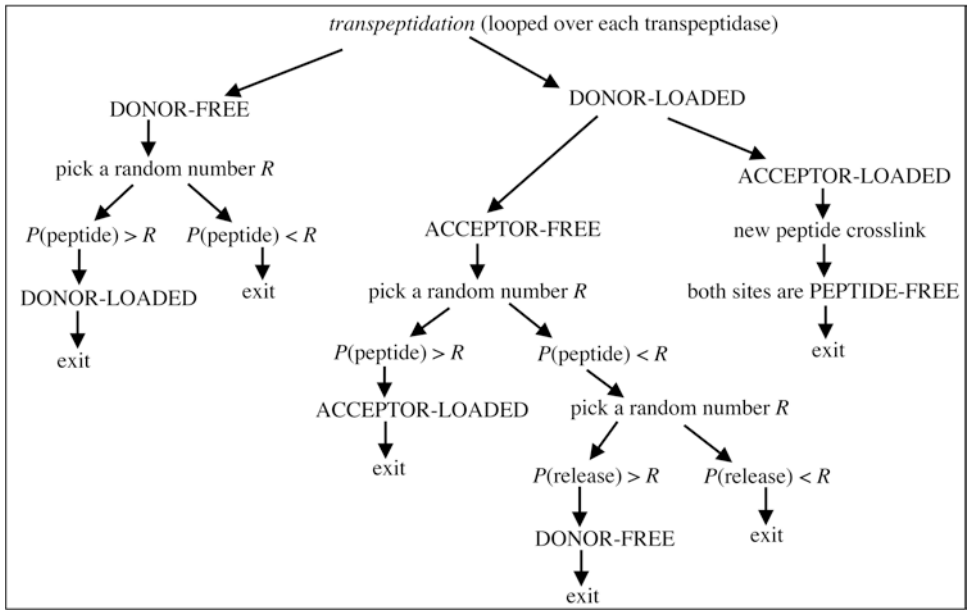

Fig. 8 Flowchart of *transpeptidation* in the simulation code. P denotes probabilities of the activities in a time step

peptide was "loaded" with (became bound to) that peptide with a probability that was a function of the distance d, $P = \left(1 - d / d_0\right)^2$. The enzyme was now DONOR-LOADED. Beyond the reaction distance, the peptide-loading probability was zero. A DONOR-LOADED transpeptidase could release the peptide (becoming DONOR-FREE again) with a smaller probability, once in 10^4 steps. If the enzyme instead loaded, with the same distance-dependent probability, an acceptor peptide as well (becoming ACCEPTOR-LOADED), a new crosslink between the corresponding beads was added to the model and the enzyme was released (becoming DONOR-FREE again) (Fig. 6). Because the fifth residues of peptides are quickly removed [73], preventing them from acting as donors, only peptides on a growing strand can be donors [1], and this restriction was implemented in our model.

3.3.3 Endopeptidation

Endopeptidases were modeled as PEPTIDE-FREE (not bound to any peptide), or PEPTIDE-BOUND (bound to one or both peptides released from crosslink cleavage). If during a time step a PEPTIDE-FREE endopeptidase diffused across a peptide crosslink, the crosslink was cleaved with a probability of 0.1 (Fig. 6), and the two peptides remained bound to the enzyme (enzyme became PEPTIDE-BOUND). In early models, the two peptides were released from the endopeptidase immediately after cleavage (enzyme became PEPTIDE-FREE). Later a "cleaved crosslink capture" hypothesis was added to the model specifying that, until competed off by transpeptidases, endopeptidases bind tightly to cleaved crosslinks (remaining PEPTIDE-BOUND), only releasing peptides (to become PEPTIDE-FREE) with a low probability, on average once every 10^7 time steps [45]. A flowchart of *endopeptidation* is presented in Fig. 9.

3.3.4 Enzyme Diffusion

Enzyme diffusion was modeled by exerting a random force on each enzyme in each time step. To generate random forces, a set of Gaussian distributed random numbers was first generated using the Box-Muller transformation [74]:

$$r_1 = \cos\left(2\pi u_2\right)\sqrt{-2\ln\left(u_1\right)} \tag{5}$$

$$r_2 = \sin\left(2\pi u_2\right)\sqrt{-2\ln\left(u_1\right)} \tag{6}$$

where u_1 and u_2 are two random numbers from a uniform 0–1 distribution. Each Cartesian component of the random force was then obtained by scaling a Gaussian random number by a force constant of 500 pN. We assumed that random forces on the small PG beads were negligible, and thus could be ignored.

3.3.5 Periplasmic Confinement

In cells, PG remodeling enzymes are confined within the thin periplasmic space. To model this confinement, the enzymes in our

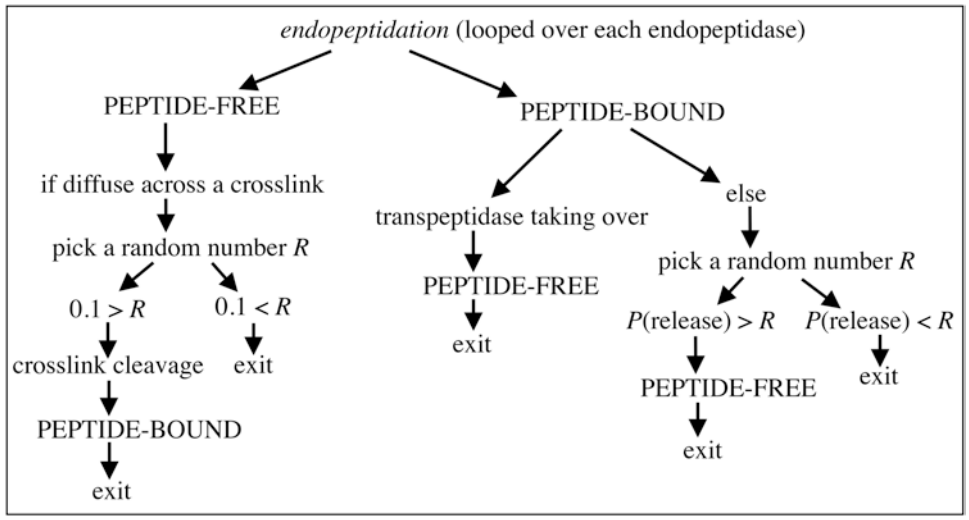

Fig. 9 Flowchart of *endopeptidation* in the simulation code. P denotes probabilities of the activities in a time step

model were constrained to the sacculus surface (Fig. 10a). As an enzyme moved a distance d_s away from the surface, a Hookean spring-like force normal to the surface was exerted on the enzyme:

$$F_{surf} = -k_{surf} d_s \tag{7}$$

where k_{surf} is a spring constant chosen as 500 pN/nm.

3.3.6 Interaction with LpoA and LpoB

In *E. coli*, the outer-membrane lipoproteins LpoA and LpoB interact with and activate the bifunctional transglycosylases PBP1A and PBP1B, which are partially embedded in the inner membrane [17, 18]. Thus active transglycosylase-lipoprotein complexes, spanning the periplasm from the outer membrane through the sacculus to the inner membrane, presumably cannot cross through strands or crosslinks. To model this constraint, as an active transglycosylase approached the edge of a hole in the network, a repulsive force was applied on the enzyme and on the two PG beads at either end of the edge (Fig. 10b). For simplicity, in calculating the repulsive force we assumed that each transglycosylase-lipoprotein complex was rigid and extended perpendicular to the sacculus surface. When the distance Δd from the enzyme's projection on the surface to the edge was less than $\Delta D = 0.5$ nm, the repulsive force was calculated as:

$$F_r = k_r \left(\frac{\Delta D}{\Delta d} - 1 \right)^2 \tag{8}$$

where $k_r = 100\text{pN}$ is a force constant.

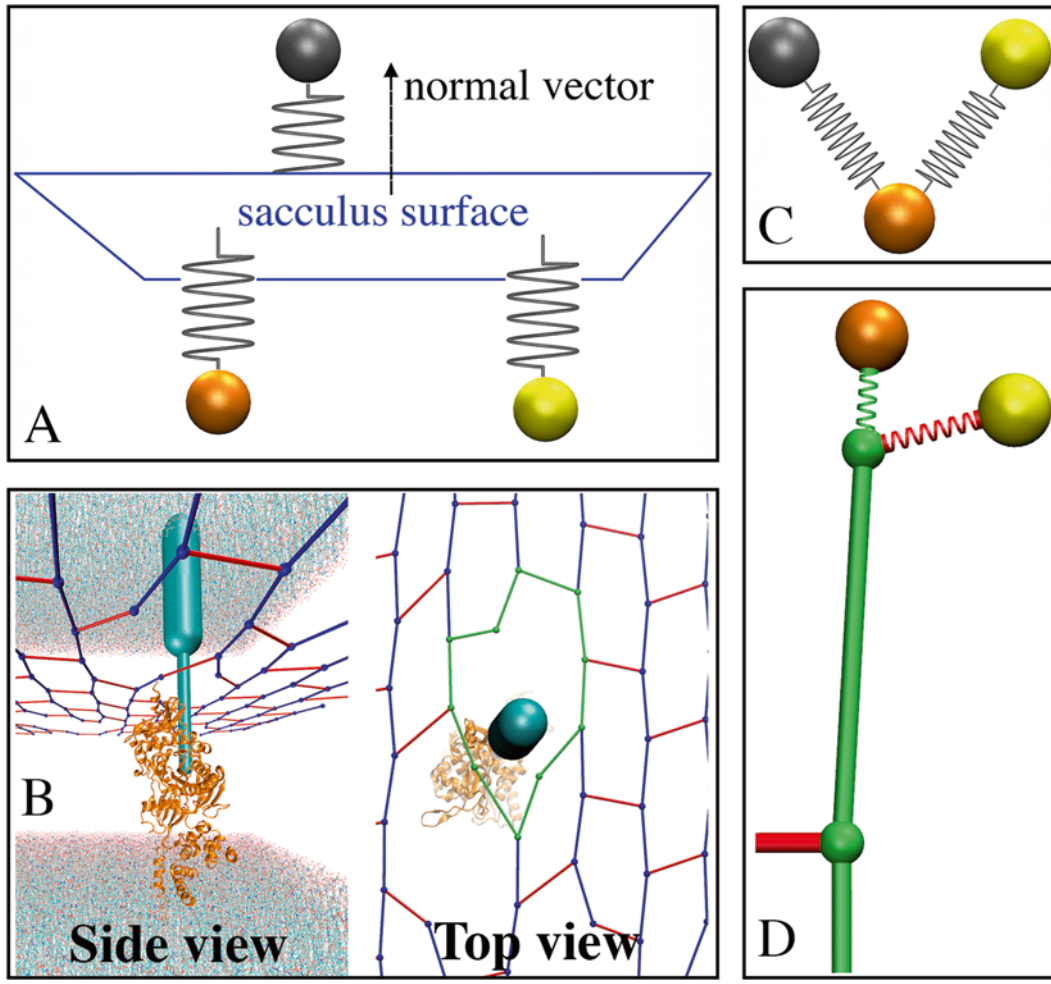

Fig. 10 Schematic of constraints on the enzymes, adapted from [45]. (**a**) The enzymes are constrained to the sacculus surface by Hookean spring-like forces. (**b**) In complex with outer membrane lipoproteins (cyan cylinder), an active transglycosylase (*orange*) is constrained within holes (*green*) formed by surrounding strands and peptide crosslinks. (**c**) In the multi-enzyme complex model, a transglycosylase is tethered to a transpeptidase (*yellow*) and an endopeptidase (*gray*) by spring-like forces. (**d**) A transglycosylase (*orange*) is linked to the tip of the growing strand by a spring-like force. An enzyme, either endopeptidase or transpeptidase (*yellow*), once bound to a peptide (*red*), is linked to the associated PG bead by a spring-like force

3.3.7 Enzyme-Enzyme Tethering

As the bifunctional transglycosylase/transpeptidases PBP1A and PBP1B are the major synthases in *E. coli* [11], in our model transglycosylases and transpeptidases were modeled as complexes in which they were linked together via a spring-like force (Fig. 10c). In the initial model, endopeptidase was not part of the complex. After a "multi-enzyme complex" hypothesis was added, transglycosylases were tethered to both transpeptidases and endopeptidases. To model enzyme tethering, if the distance d_{cz} between two tethered enzymes became larger than $D_0 = 1.0\text{nm}$, a spring-like force was applied to draw them closer together:

$$F_{cz} = -k_{cz}\left(d_{cz} - D_0\right) \tag{9}$$

where $k_{cz} = 10\text{pN} / \text{nm}$ is a force constant.

3.3.8 Enzyme-PG Interaction

We also modeled binding of enzymes to PG while they remodeled the sacculus (Fig. 10d). As a transglycosylase was elongating a new strand, the enzyme was linked to the PG bead at the strand tip via a spring (called a G-spring) of constant $k_{gt} = 50\text{pN} / nm$ and relaxed length $d_{gt} = 0.5\text{nm}$. The bending stiffness of glycan was taken into account at the tip using Eq. 1 with θ now representing the angle between the G-spring and the strand. Enzymes also transiently bound peptides. For instance, transpeptidases bound to peptides before crosslinking them, and endopeptidases might remain bound to peptides released from cleaved crosslinks. To model the binding of peptides to an enzyme, a restoring force $F_{pt} = -k_{pt}\left(d - d_{pt}\right)$, where $k_{pt} = 50\text{pN} / \text{nm}$, was applied to both the enzyme and the peptide-associated PG bead if the distance d between them was more than $d_{pt} = 1.0\text{nm}$. Within distance d_{pt}, the force was zero.

3.4 Relaxation

To relax sacculi after initial generation and during growth we used a simple MD simulation of the coarse-grained model. Specifically, coordinate $X(t)$ of each bead was evolved following the Langevin equation:

$$M\frac{d^2X}{dt^2} = -\nabla U\left(X\right) - \gamma\frac{dX}{dt} + R\left(t\right) \tag{10}$$

where M is the mass of the bead, U the interaction potential, γ the damping constant and R the random force on the bead. Assuming inertia of the bead was negligible, and thus $M = 0$, displacement was therefore simply a linear function of force:

$$dX = \frac{1}{\gamma}\left[-\nabla U\left(X\right) + R\right]dt \tag{11}$$

In principle, one might be able to estimate viscous drag coefficients from the masses and sizes of the PG beads and enzymes. However, since sacculi are linked to the outer membrane through lipoproteins [75, 76], and since PBPs might exist in complexes with other proteins such as MreBCD, RodA, or RodZ [77], their response to viscosity might differ. For simplicity, the effective viscous drag coefficients of the enzymes were estimated to be four times that of the PG beads.

Using a fixed time step could make the system unstable because a large force might move a bead too far. To prevent this instability, we constrained the maximal displacement of the PG beads, corresponding to the maximal force F_{max}, in every time step, to $D_{max} = 0.005$ nm. Displacement D of each bead was then calculated as

$$D = \frac{D_{max}}{\gamma F_{max}} F \tag{12}$$

where F is the force on the bead, and $\gamma = 1.0$ for PG beads and 4.0 for enzymes.

3.5 Shape Characterization

We developed measures to quantify preservation of sacculus integrity and maintenance of rod shape. First, we calculated hole size since large holes in the sacculus could threaten cell integrity. We then quantified bulges, straightness, and roughness of the sacculus surface to analyze rod shape maintenance.

3.5.1 Hole Size

We quantified hole size by calculating the surface area covering the hole. A hole on the sacculus surface is a polygon whose edges connect neighboring beads into a closed loop that cannot be further divided by a glycan or peptide bond (Fig. 5). This polygon was divided into triangles sharing the polygon's center as their third vertex. The hole size was then calculated as the sum of the triangles' areas.

3.5.2 Central Line

To characterize maintenance of rod shape, we first had to define a central line through the sacculus between the polar caps. To do this, we constructed a central "axis" chain of beads extending the length of the cylinder, connected by unstretched springs of uniform spring constant. This axis chain was then connected to the sacculus by dividing the PG cylinder into segments, each corresponding to one axis bead, and connecting each axis bead to the PG beads in its corresponding segment with identical springs. The axis chain was relaxed by minimizing the energy

$$E = \sum \frac{1}{2} k_b \left(d_{ij} - d_0 \right)^2 + \sum \frac{1}{2} k_\theta \left(\theta_i - \theta_0 \right)^2 + \sum \frac{1}{2} k_{pg} l_{ij}^{\ 2} \tag{13}$$

The first term represents the axis springs, where dij is the distance between axis bead i and axis bead j, $k_b = 10^3\,\mathrm{pN/nm}$, and $d_0 = 2.0$ nm. The second term represents the bending stiffness of the axis chain, where θi is the angle at axis bead i, $k_\theta = 10^{-20}$ J, and $\theta_0 = 3.14$ rad. The third term represents the springs connecting the axis beads to the sacculus, where lij is the distance between axis bead i and PG bead j, and $k_{pg} = 10^{-2}\,\mathrm{pN/nm}$. The central line was then defined as this relaxed axis chain.

3.5.3 Bulges

To quantify bulges we assessed fluctuations in local radii. The PG cylinder was divided into short segments, and each local radius was calculated as the average distance from the PG beads of that segment to the central line.

3.5.4 Straightness

Sacculus straightness was defined as the ratio of the shortest distance between the end points of the central line to its contour length.

3.5.5 Roughness

Surface roughness was defined as the ratio of standard deviation to mean of the local radii.

3.6 Visualization of Sacculus Growth

Simulation codes were written in Fortran. Visualization of sacculus growth using Visual Molecular Dynamics (VMD) [54], however, was a challenge. Sacculus growth involved addition of new beads, cleavage of old bonds, and formation of new ones, but VMD could only visualize systems with constant numbers of beads and identical topology. To overcome this problem, the following two strategies were applied.

First, to ensure a constant number of beads, the number of "future" PG beads was predicted and their coordinates were initially set to be at the center of the sacculus, forming a reservoir of available beads. Once a bead was "added," its coordinates were simply changed to match the location of the corresponding enzyme, and then evolved as part of the dynamic system using Eq. 12.

The second problem was maintaining topology. Due to the mesh-like nature of the PG network, many bonds, either glycan or peptide, were formed on common beads, so that bond cleavage and formation violated the topological constraint. To overcome this problem, instead of using one visualization bead (V-bead) to visualize one PG bead, a bonded pair of V-beads (blue = existing glycan, green = new glycan, red = peptide) was used to visualize each glycan/peptide bond. Thus, a PG bead at the junction of N bonds was visualized with N V-beads overlapping one another, ensuring that each bond could be added/removed independently from the others. So, for example, when a new peptide bond was added, two bonded V-peptide-beads were moved from the central reservoir to the location of the corresponding PG beads of the bond. When a new glycan bead was added, two bonded V-glycan-beads were moved from the central reservoir to the location of the new bond, one overlapping the existing bead at the strand tip and the other forming the new strand tip. To visualize removal of a glycan bead or peptide bond, the corresponding V-glycan/peptide-beads were moved back to the central reservoir. A schematic of visualization is presented in Fig. 11.

To show a dynamic process like sacculus growth, moving images obviously work better than static ones. We therefore created movies to document simulated sacculus growth events, analysis of causes of shape loss, and hypothetical mechanisms to fix problems [45]. To generate movies, we first captured individual snapshots of sacculus remodeling using VMD. Text and graphical schematics were then embedded using Photoshop. Frames were imported into QuickTime Pro to generate individual movies, and Final Cut Pro used to concatenate movies.

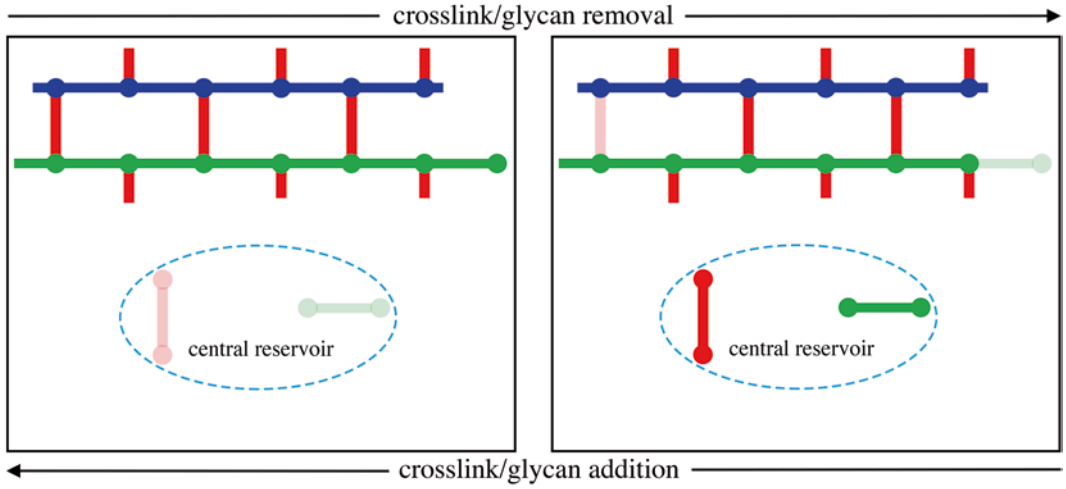

Fig. 11 Schematic showing the use of visualization beads (shown in central reservoir) to show the addition/removal of PG beads or peptide crosslinks. Existing PG is visualized in *blue*, new PG in *green*, and peptides in *red*

4 Notes

1. In the first round of our work, we used our model to reveal many challenges the cell might face while remodeling its wall, as well as possible molecular mechanisms the cell might use to preserve its integrity and characteristic rod shape during cell elongation [45]. We highlight some of the results of our simulations here.

   First and foremost, as hydrolases must cleave peptide bonds in order for new PG material to be incorporated, their activities must be regulated to preserve sacculus integrity in the presence of large internal turgor pressure. We have shown that not only do synthases and hydrolases likely form a complex, but their activities are likely temporally coordinated in such a way that a peptide released by bond cleavage would be captured quickly by new crosslink formation. Second, activities of synthases are also likely regulated spatially and temporally to prevent aggregation of new material. To ensure processivity, not only might the orientation of transglycosylases be fixed, but their translocation along the new glycan strand might also be facilitated by transpeptidation. Further, termination of transglycosylase is likely not purely stochastic but rather regulated, for instance by crosslinkage of the growing strand and/or by hole size. Interestingly, we found that the presence of a housekeeping glycosidase that removes uncrosslinked glycan tails could help prevent aggregation. While our manuscript was under revision, such a glycosidase was identified in cells [78], proving the usefulness of our approach in generating testable biological hypotheses.

Maintenance of rod shape requires maintenance of regular order of glycan strands, since disordered PG leads to bulges and shape distortion. We have shown that the presence of multiple synthases in the complex could help preserve the regular order and shape of the sacculus. While bifunctional transpeptidases likely form crosslinks only on one side, the presence of a monofunctional transpeptidase would ensure crosslink formation on the other side of new strands, perhaps explaining why the monofunctional PBP2 of *E. coli* is essential for shape maintenance [79]. Finally, in a single-strand insertion mode, new peptides do not line up with old peptides, causing circumferential stress and, gradually, distortion. By contrast, we show that the presence of two transglycosylases incorporating two strands into the sacculus concomitantly brings the peptides into register, thus preventing defects.

Our results show that rod shape maintenance can occur with only local coordination of the enzymes within individual, randomly diffusing complexes, and that coordination of PG insertion sites over long distances by cytoskeletal filament scaffolds, a role previously suggested for MreB, is not required.

2. In the future, it will be interesting to expand our model to include cytoplasmic proteins that regulate PG synthesis, notably MreB during cell elongation and FtsZ during division [77]. Several roles have been proposed for MreB including serving as a cytoskeletal scaffold to direct PG insertion sites [27, 44] and/or simply tagging along [23, 24, 28], bridging cytoplasmic and periplasmic enzymes [45, 80], and organizing and/or orienting the PG remodeling enzyme complex [45]. To test whether MreB directs PG insertion sites, as in the Huang model, insertion of new strands could be constrained to sites that implicitly represent the location of MreB [28, 41, 43, 44]. To test whether MreB helps form the PG remodeling complex by channeling PG precursors and/or organizing the enzymes, the presence/absence of MreB could be represented by a high/low probability of loading precursors onto transglycosylases and/or a long/short lifetime of the complex.

   It has been proposed that FtsZ may serve as a scaffold to recruit divisome proteins and/or exert a constricting force on the membrane during division [81]. To model the former, the localization of PG synthesis enzymes could simply be biased to the midcell. To model the latter, assuming that forces exerted on the membrane would be transferred to the stress-bearing sacculus, forces perpendicular to the sacculus surface could be applied to PG beads at sites representing the location of FtsZ.

   We plan to use the same method to study many related topics, including, for example, shape maintenance of Gram-positive bacteria, lemon-to-rod transition and rod shape recovery, cell

division, and even sporulation, where PG synthesis/hydrolysis is thought to drive prespore engulfment [82–84].

3. We originally adopted the spring model for peptide crosslinks from the work of Huang et al. [44]. This model, however, failed to stabilize the system if the diameter of the sacculus was large or there were big holes on the surface. As the sacculus diameter increased, the cross-sectional area of the sacculus and therefore the stress on peptide crosslinks from turgor pressure increased quadratically, while the number of crosslinks along the circumference increased only linearly. As the sacculus reached a certain diameter, the system therefore became unstable, preventing realistic representation of the sacculus' mechanical properties and exploration of the effect of size.
4. In simulating a sacculus four times larger, to reduce the computational cost only the cylindrical part of the sacculus was modeled, without including the two caps. In the other simulations, PG synthesis was not modeled to occur at the caps due to experimental evidence that the caps are inert, so this should not affect the conclusions in any way.

Acknowledgements

The authors wish to thank Catherine Oikonomou for revising the manuscript for clarity.

References

1. Höltje JV (1998) Growth of the stress-bearing and shape-maintaining murein sacculus of Escherichia coli. Microbiol Mol Biol Rev 62:181–203
2. Primosigh J, Pelzer H, Maass D, Weidel W (1961) Chemical characterization of mucopeptides released from the E. coli B cell wall by enzymic action. Biochim Biophys Acta 46:68–80
3. Glauner B (1988) Separation and quantification of muropeptides with high-performance liquid chromatography. Anal Biochem 172:451–464. doi:10.1016/0003-2697(88)90468-X
4. Harz H, Burgdorf K, Höltje J-V (1990) Isolation and separation of the glycan strands from murein of Escherichia coli by reversed-phase high-performance liquid chromatography. Anal Biochem 190:120–128. doi:10.1016/0003-2697(90)90144-X
5. Weidel W, Pelzer H (1964) Bagshaped macromolecules—a new outlook on bacterial cell walls. Adv Enzymol Relat Areas Mol Biol 26: 193–232
6. Gan L, Chen S, Jensen GJ (2008) Molecular organization of Gram-negative peptidoglycan. Proc Natl Acad Sci 105:18953–18957. doi:10.1073/pnas.0808035105
7. Barreteau H, Kovac A, Boniface A et al (2008) Cytoplasmic steps of peptidoglycan biosynthesis. FEMS Microbiol Rev 32:168–207. doi:10.1111/j.1574-6976.2008.00104.x
8. Sauvage E, Kerff F, Terrak M et al (2008) The penicillin-binding proteins: structure and role in peptidoglycan biosynthesis. FEMS Microbiol Rev 32:234–258. doi:10.1111/j.1574-6976.2008.00105.x
9. Singh SK, SaiSree L, Amrutha RN, Reddy M (2012) Three redundant murein endopeptidases catalyse an essential cleavage step in peptidoglycan synthesis of Escherichia coliK12. Mol Microbiol 86:1036–1051. doi:10.1111/mmi.12058
10. Sung M-T, Lai Y-T, Huang C-Y et al (2009) Crystal structure of the membrane-bound bifunctional transglycosylase PBP1b from

Escherichia coli. Proc Natl Acad Sci U S A 106: 8824–8829. doi:10.1073/pnas.0904030106

11. Vollmer W, Bertsche U (2008) Murein (peptidoglycan) structure, architecture and biosynthesis in Escherichia coli. Biochim Biophys Acta 1778:1714–1734, doi: 16/j.bbamem.2007.06.007
12. Banzhaf M, van den Berg van Saparoea B, Terrak M et al (2012) Cooperativity of peptidoglycan synthases active in bacterial cell elongation. Mol Microbiol 85:179–194. doi:10.1111/j.1365-2958.2012.08103.x
13. Romeis T, Höltje JV (1994) Specific interaction of penicillin-binding proteins 3 and 7/8 with soluble lytic transglycosylase in Escherichia coli. J Biol Chem 269:21603–21607
14. von Rechenberg M, Ursinus A, Höltje JV (1996) Affinity chromatography as a means to study multienzyme complexes involved in murein synthesis. Microb Drug Resist 2:155–157
15. Vollmer W, von Rechenberg M, Holtje J-V (1999) Demonstration of molecular interactions between the murein polymerase PBP1B, the lytic transglycosylase MltA, and the scaffolding protein MipA of Escherichia coli. J Biol Chem 274:6726–6734. doi:10.1074/jbc.274.10.6726
16. Bertsche U, Kast T, Wolf B et al (2006) Interaction between two murein (peptidoglycan) synthases, PBP3 and PBP1B, in Escherichia coli. Mol Microbiol 61:675–690. doi:10.1111/j.1365-2958.2006.05280.x
17. Paradis-Bleau C, Markovski M, Uehara T et al (2010) Lipoprotein cofactors located in the outer membrane activate bacterial cell wall polymerases. Cell 143:1110–1120. doi:10.1016/j.cell.2010.11.037
18. Typas A, Banzhaf M, van den Berg van Saparoea B et al (2010) Regulation of peptidoglycan synthesis by outer-membrane proteins. Cell 143:1097–1109. doi:10.1016/j.cell.2010.11.038
19. Divakaruni AV, Loo RRO, Xie Y et al (2005) The cell-shape protein MreC interacts with extracytoplasmic proteins including cell wall assembly complexes in Caulobacter crescentus. Proc Natl Acad Sci U S A 102:18602–18607. doi:10.1073/pnas.0507937102
20. van den Ent F, Leaver M, Bendezu F et al (2006) Dimeric structure of the cell shape protein MreC and its functional implications. Mol Microbiol 62:1631–1642. doi:10.1111/j.1365-2958.2006.05485.x
21. White CL, Kitich A, Gober JW (2010) Positioning cell wall synthetic complexes by the bacterial morphogenetic proteins MreB and MreD. Mol Microbiol 76:616–633. doi:10.1111/j.1365-2958.2010.07108.x
22. Dye NA, Pincus Z, Theriot JA et al (2005) Two independent spiral structures control cell shape in Caulobacter. Proc Natl Acad Sci U S A 102:18608–18613. doi:10.1073/pnas.0507708102
23. Domínguez-Escobar J, Chastanet A, Crevenna AH et al (2011) Processive movement of MreB-associated cell wall biosynthetic complexes in bacteria. Science 333:225–228. doi:10.1126/science.1203466
24. Garner EC, Bernard R, Wang W et al (2011) Coupled, circumferential motions of the cell wall synthesis machinery and MreB filaments in B. subtilis. Science 333:222–225. doi:10.1126/science.1203285
25. Lee TK, Tropini C, Hsin J et al (2014) A dynamically assembled cell wall synthesis machinery buffers cell growth. Proc Natl Acad Sci 201313826. doi: 10.1073/pnas.1313826111
26. Koch AL (1990) Additional arguments for the key role of "smart" autolysins in the enlargement of the wall of gram-negative bacteria. Res Microbiol 141:529–541
27. Jones LJF, Carballido-López R, Errington J (2001) Control of cell shape in bacteria: helical, actin-like filaments in Bacillus subtilis. Cell 104:913–922, doi: 16/S0092-8674(01)00287-2
28. van Teeffelen S, Wang S, Furchtgott L et al (2011) The bacterial actin MreB rotates, and rotation depends on cell-wall assembly. Proc Natl Acad Sci 108:15822–15827. doi:10.1073/pnas.1108999108
29. Daniel RA, Errington J (2003) Control of cell morphogenesis in bacteria: two distinct ways to make a rod-shaped cell. Cell 113:767–776, doi: 16/S0092-8674(03)00421-5
30. Kruse T, Møller-Jensen J, Løbner-Olesen A, Gerdes K (2003) Dysfunctional MreB inhibits chromosome segregation in Escherichia coli. EMBO J 22:5283–5292. doi:10.1093/emboj/cdg504
31. Shih Y-L, Le T, Rothfield L (2003) Division site selection in Escherichia coli involves dynamic redistribution of Min proteins within coiled structures that extend between the two cell poles. Proc Natl Acad Sci 100:7865–7870. doi:10.1073/pnas.1232225100
32. Soufo HJD, Graumann PL (2003) Actin-like proteins MreB and Mbl from Bacillus subtilis are required for bipolar positioning of replication origins. Curr Biol 13:1916–1920. doi:10.1016/j.cub.2003.10.024
33. Soufo HJD, Graumann PL (2004) Dynamic movement of actin-like proteins within bacterial cells. EMBO Rep 5:789–794. doi:10.1038/sj.embor.7400209

34. Figge RM, Divakaruni AV, Gober JW (2004) MreB, the cell shape-determining bacterial actin homologue, co-ordinates cell wall morphogenesis in Caulobacter crescentus. Mol Microbiol 51:1321–1332. doi:10.1111/j.1365-2958.2003.03936.x
35. Gitai Z, Dye N, Shapiro L (2004) An actin-like gene can determine cell polarity in bacteria. Proc Natl Acad Sci U S A 101:8643–8648. doi:10.1073/pnas.0402638101
36. Vats P, Rothfield L (2007) Duplication and segregation of the actin (MreB) cytoskeleton during the prokaryotic cell cycle. Proc Natl Acad Sci 104:17795–17800. doi:10.1073/pnas.0708739104
37. Swulius MT, Chen S, Jane Ding H et al (2011) Long helical filaments are not seen encircling cells in electron cryotomograms of rod-shaped bacteria. Biochem Biophys Res Commun 407:650–655. doi:10.1016/j.bbrc.2011.03.062
38. Swulius MT, Jensen GJ (2012) The helical MreB cytoskeleton in Escherichia coli MC1000/pLE7 is an artifact of the N-terminal yellow fluorescent protein tag. J Bacteriol 194:6382–6386. doi:10.1128/JB.00505-12
39. Reimold C, Defeu Soufo HJ, Dempwolff F, Graumann PL (2013) Motion of variable-length MreB filaments at the bacterial cell membrane influences cell morphology. Mol Biol Cell 24:2340–2349. doi:10.1091/mbc.E12-10-0728
40. Olshausen PV, Defeu Soufo HJ, Wicker K et al (2013) Superresolution imaging of dynamic MreB filaments in B. subtilis—a multiple-motor-driven transport? Biophys J 105:1171–1181. doi:10.1016/j.bpj.2013.07.038
41. Ursell TS, Nguyen J, Monds RD et al (2014) Rod-like bacterial shape is maintained by feedback between cell curvature and cytoskeletal localization. Proc Natl Acad Sci 111:E1025–E1034. doi:10.1073/pnas.1317174111
42. Huang KC, Mukhopadhyay R, Wen B et al (2008) Cell shape and cell-wall organization in Gram-negative bacteria. Proc Natl Acad Sci 105:19282–19287. doi:10.1073/pnas.0805309105
43. Wang S, Furchtgott L, Huang KC, Shaevitz JW (2012) Helical insertion of peptidoglycan produces chiral ordering of the bacterial cell wall. Proc Natl Acad Sci 109:E595–E604. doi:10.1073/pnas.1117132109
44. Furchtgott L, Wingreen NS, Huang KC (2011) Mechanisms for maintaining cell shape in rod-shaped Gram-negative bacteria. Mol Microbiol 81:340–353. doi:10.1111/j.1365-2958.2011.07616.x
45. Nguyen LT, Gumbart JC, Beeby M, Jensen GJ (2015) Coarse-grained simulations of bacterial cell wall growth reveal that local coordination alone can be sufficient to maintain rod shape. Proc Natl Acad Sci 112:E3689–E3698. doi:10.1073/pnas.1504281112
46. Höltje J-V (1996) A hypothetical holoenzyme involved in the replication of the murein sacculus of Escherichia Coli. Microbiology 142:1911–1918. doi:10.1099/13500872-142-8-1911
47. Cooper S, Hsieh ML, Guenther B (1988) Mode of peptidoglycan synthesis in Salmonella typhimurium: single-strand insertion. J Bacteriol 170:3509–3512
48. de Jonge BL, Wientjes FB, Jurida I et al (1989) Peptidoglycan synthesis during the cell cycle of Escherichia coli: composition and mode of insertion. J Bacteriol 171:5783–5794
49. Burman LG, Park JT (1984) Molecular model for elongation of the murein sacculus of Escherichia coli. Proc Natl Acad Sci U S A 81:1844–1848
50. Zijderveld CA, Aarsman ME, den Blaauwen T, Nanninga N (1991) Penicillin-binding protein 1B of Escherichia coli exists in dimeric forms. J Bacteriol 173:5740–5746
51. Charpentier X, Chalut C, Rémy M-H, Masson J-M (2002) Penicillin-binding proteins 1a and 1b form independent dimers in Escherichia coli. J Bacteriol 184:3749–3752. doi:10.1128/JB.184.13.3749-3752.2002
52. Bertsche U, Breukink E, Kast T, Vollmer W (2005) In vitro murein peptidoglycan synthesis by dimers of the bifunctional transglycosylase-transpeptidase PBP1B from Escherichia coli. J Biol Chem 280:38096–38101. doi:10.1074/jbc.M508646200
53. Zhao G, Perilla JR, Yufenyuy EL et al (2013) Mature HIV-1 capsid structure by cryo-electron microscopy and all-atom molecular dynamics. Nature 497:643–646. doi:10.1038/nature12162
54. Burge RE, Fowler AG, Reaveley DA (1977) Structure of the peptidoglycan of bacterial cell walls. J Mol Biol 117:927–953. doi:10.1016/S0022-2836(77)80006-5
55. Labischinski H, Barnickel G, Bradaczek H, Giesbrecht P (1979) On the secondary and tertiary structure of murein. Eur J Biochem 95:147–155.doi:10.1111/j.1432-1033.1979.tb12949.x
56. Kim SJ, Singh M, Preobrazhenskaya M, Schaefer J (2013) Staphylococcus aureus peptidoglycan stem packing by rotational-echo double resonance NMR spectroscopy. Biochemistry (Mosc) 52:3651–3659. doi:10.1021/bi4005039
57. Beeby M, Gumbart JC, Roux B, Jensen GJ (2013) Architecture and assembly of the Gram-positive cell wall. Mol Microbiol 88:664–672. doi:10.1111/mmi.12203
58. Gumbart JC, Beeby M, Jensen GJ, Roux B (2014) Escherichia coli peptidoglycan structure

and mechanics as predicted by atomic-scale simulations. PLoS Comput Biol 10, e1003475. doi:10.1371/journal.pcbi.1003475

59. Phillips JC, Braun R, Wang W et al (2005) Scalable molecular dynamics with NAMD. J Comput Chem 26:1781–1802. doi:10.1002/jcc.20289
60. Darve E, Pohorille A (2001) Calculating free energies using average force. J Chem Phys 115:9169–9183. doi:10.1063/1.1410978
61. Hénin J, Chipot C (2004) Overcoming free energy barriers using unconstrained molecular dynamics simulations. J Chem Phys 121:2904–2914. doi:10.1063/1.1773132
62. Braun V, Gnirke H, Henning U, Rehn K (1973) Model for the structure of the shape-maintaining layer of the Escherichia coli cell envelope. J Bacteriol 114:1264–1270
63. Reed RH, Walsby AE (1985) Changes in turgor pressure in response to increases in external NaCl concentration in the gas-vacuolate cyanobacterium Microcystis sp. Arch Microbiol 143:290–296. doi:10.1007/BF00411252
64. Koch AL, Pinette MF (1987) Nephelometric determination of turgor pressure in growing gram-negative bacteria. J Bacteriol 169:3654
65. Cayley DS, Guttman HJ, Record MT (2000) Biophysical characterization of changes in amounts and activity of Escherichia coli cell and compartment water and turgor pressure in response to osmotic stress. Biophys J 78:1748–1764
66. Lovering AL, De Castro LH, Lim D, Strynadka NCJ (2007) Structural insight into the transglycosylation step of bacterial cell-wall biosynthesis. Science 315:1402–1405. doi:10.1126/science.1136611
67. Yuan Y, Barrett D, Zhang Y et al (2007) Crystal structure of a peptidoglycan glycosyltransferase suggests a model for processive glycan chain synthesis. Proc Natl Acad Sci 104:5348–5353. doi:10.1073/pnas.0701160104
68. Perlstein DL, Wang T-SA, Doud EH et al (2010) The role of the substrate lipid in processive glycan polymerization by the peptidoglycan glycosyltransferases. J Am Chem Soc 132:48–49. doi:10.1021/ja909325m
69. Wise EM, Park JT (1965) Penicillin: its basic site of action as an inhibitor of a peptide cross-linking reaction in cell wall mucopeptide synthesis. Proc Natl Acad Sci U S A 54:75–81
70. Tipper DJ, Strominger JL (1965) Mechanism of action of penicillins: a proposal based on their structural similarity to acyl-D-alanyl-D-alanine. Proc Natl Acad Sci U S A 54:1133–1141
71. Ghuysen JM (1997) Penicillin-binding proteins. Wall peptidoglycan assembly and resistance to penicillin: facts, doubts and hopes. Int J Antimicrob Agents 8:45–60
72. de Pedro MA, Schwarz U (1981) Heterogeneity of newly inserted and preexisting murein in the sacculus of Escherichia coli. Proc Natl Acad Sci U S A 78:5856–5860
73. Box GEP, Muller ME (1958) A note on the generation of random normal deviates. Ann Math Stat 29:610–611. doi:10.1214/aoms/1177706645
74. Braun V (1975) Covalent lipoprotein from the outer membrane of Escherichia coli. Biochim Biophys Acta 415:335–377
75. Silhavy TJ, Kahne D, Walker S (2010) The bacterial cell envelope. Cold Spring Harb Perspect Biol. doi:10.1101/cshperspect.a000414
76. Typas A, Banzhaf M, Gross CA, Vollmer W (2012) From the regulation of peptidoglycan synthesis to bacterial growth and morphology. Nat Rev Micro 10:123–136. doi:10.1038/nrmicro2677
77. Humphrey W, Dalke A, Schulten K (1996) VMD: visual molecular dynamics. J Mol Graph 14:33–38. doi:10.1016/0263-7855(96)00018-5
78. Cho H, Uehara T, Bernhardt TG (2014) Beta-lactam antibiotics induce a lethal malfunctioning of the bacterial cell wall synthesis machinery. Cell 159:1300–1311. doi:10.1016/j.cell.2014.11.017
79. Spratt BG (1975) Distinct penicillin binding proteins involved in the division, elongation, and shape of Escherichia coli K12. Proc Natl Acad Sci U S A 72:2999–3003
80. Rueff A-S, Chastanet A, Domínguez-Escobar J et al (2014) An early cytoplasmic step of peptidoglycan synthesis is associated to MreB in Bacillus subtilis. Mol Microbiol 91:348–362. doi:10.1111/mmi.12467
81. Erickson HP, Anderson DE, Osawa M (2010) FtsZ in bacterial cytokinesis: cytoskeleton and force generator all in one. Microbiol Mol Biol Rev 74:504–528. doi:10.1128/MMBR.00021-10
82. Meyer P, Gutierrez J, Pogliano K, Dworkin J (2010) Cell wall synthesis is necessary for membrane dynamics during sporulation of Bacillus subtilis. Mol Microbiol 76:956–970. doi:10.1111/j.1365-2958.2010.07155.x
83. Tocheva EI, Matson EG, Morris DM et al (2011) Peptidoglycan remodeling and conversion of an inner membrane into an outer membrane during sporulation. Cell 146:799–812. doi:10.1016/j.cell.2011.07.029
84. Tocheva EI, López-Garrido J, Hughes HV et al (2013) Peptidoglycan transformations during Bacillus subtilis sporulation. Mol Microbiol 88:673–686. doi:10.1111/mmi.12201
85. Powell AJ, Tomberg J, Deacon AM et al (2009) Crystal structures of penicillin-binding

protein 2 from penicillin-susceptible and -resistant strains of Neisseria gonorrhoeae reveal an unexpectedly subtle mechanism for antibiotic resistance. J Biol Chem 284:1202–1212. doi:10.1074/jbc.M805761200

86. Kishida H, Unzai S, Roper DI et al (2006) Crystal structure of penicillin binding protein 4 (dacB) from Escherichia coli, both in the native form and covalently linked to various antibiotics. Biochemistry (Mosc) 45:783–792. doi:10.1021/bi051533t